Received March 30, 2021, accepted April 16, 2021, date of publication April 26, 2021, date of current version May 7, 2021.

Digital Object Identifier 10.1109/ACCESS.2021.3075660

Design and Testing of a Helix Antenna Deployment System for a 1U CubeSat

MIQUEL SUREDA[1,2,3], MARCO SOBRINO[1], ORIOL MILLAN[1], ANDREA AGUILELLA[1], ARNAU SOLANELLAS[1], MARC BADIA[1], JOAN FRANCESC MUNOZ-MARTIN[1,2], LARA FERNANDEZ[1,2,4], (Student Member, IEEE), JOAN A. RUIZ-DE-AZUA[1,2,4], (Member, IEEE), AND ADRIANO CAMPS[1,2]

[1]CommSensLab, Department of Signal Theory and Communications, UPC BarcelonaTech, 08034 Barcelona, Spain
[2]Space Science and Technology Research Group, Institute of Space Studies of Catalonia (IEEC), CTE/UPC, 08034 Barcelona, Spain
[3]Department of Physics, UPC BarcelonaTech, 08034 Barcelona, Spain
[4]Department of Network Engineering, UPC BarcelonaTech, 08034 Barcelona, Spain

Corresponding author: Miquel Sureda (miquel.sureda@upc.edu)

ABSTRACT CubeSats have revolutionized Earth Observation and space science, although their small size severely restricts satellite performance and payload. Antenna deployment from a stowed configuration in these small-satellites remains a great challenge. This paper presents the design, optimization, and testing of an L-band helix antenna deployment system for the ^{3}Cat-4, a 1U CubeSat developed at the NanoSat Lab (UPC). The 506-mm-long antenna is packed into a 26.8 mm gap together with a tip mass that provides a gravity gradient for nadir-pointing. The ^{3}Cat-4 Nadir Antenna Deployment Subsystem (NADS) melts dyneema strings to release the antenna in successive steps. PTFE coated fiberglass ensures the helix's nominal diameter and pitch while a security locking mechanism serves as a redundant system for holding it in place before deploying. Our novel methodology optimizes the number and length of the NADS deployment steps. A slow-motion camera and image recognition software track the velocity and acceleration of the antenna sections by means of tracking dots. Kinematic analysis of the antenna resulted in a final design of four length steps: 90, 300, 420 and 506 mm. Our methodology for calculating these values can be widely applied for measuring many deployment system's kinematic properties. The NADS performance is tested by characterizing antenna rigidity, analyzing helix behavior after one year in stowed configuration, and by testing the deployment mechanism in a thermal vacuum chamber at −35°C, the most critical temperature stress scenario. All test results are satisfactory. The final design of the NADS deployment mechanism is light, stable, reliable, affordable, highly scalable, and can be used in many antenna configurations and geometries. The ^{3}Cat-4 mission was selected by the ESA Academy to be launched in Q4 2021.

INDEX TERMS CubeSat, new space, deployable antenna, helical antenna.

I. INTRODUCTION

In recent years, CubeSats have become the spearhead of new space technologies. This nanosatellite platform was initially conceived as an affordable means for students to build and fly a spacecraft, but it recently became an important tool for new space-based business models. The subsequent great boom in CubeSats resulted from platform standardization, continued progress in technology miniaturization, and Commercial Off-The-Shelf (COTS) [1]. However, antenna deployment on CubeSats remains challenging due to their restricted dimensions, and this has forced designers to develop new deployment systems for antennas that are stowed inside the small satellites during launch and deployed from the platform once in orbit.

This challenge is amplified by the requirements of designing high-gain antennas. While several high-gain antenna concepts have been proposed for CubeSats, none have obtained optimum performance [2]. Patch antennas are easy to integrate on flat surfaces like the sides of a CubeSat, but these can provide only medium gain in 1U or 2U configurations, due to their size restrictions. Reflector antennas achieve higher gain while delivering faster communications and data downloads, but they are difficult to integrate and deploy on small satellites [3]. Helix antennas provide considerable gain with natural circular polarization and wide bandwidth [4]. However,

The associate editor coordinating the review of this manuscript and approving it for publication was Zheng H. Zhu.

This work is licensed under a Creative Commons Attribution-NonCommercial-NoDerivatives 4.0 License.
For more information, see https://creativecommons.org/licenses/by-nc-nd/4.0/

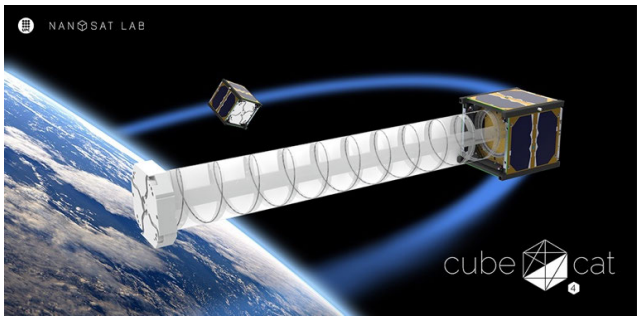

FIGURE 1. Rendering of the 1U CubeSat ^{3}Cat-4 orbiting the Earth in its stowed and deployed configurations. Source: NanoSat Lab website.

their deployment system poses enormous design challenges, especially when the antenna length exceeds the CubeSat's dimensions.

This is the case for the Nadir Antenna that we have developed at the NanoSat Lab (UPC). The Nadir Antenna is an L-Band helix antenna incorporated into a 1-Unit (1U) CubeSat [5] named ^{3}Cat-4. The ^{3}Cat-4 mission aims to demonstrate the technological capabilities of a 1U CubeSat when performing dual-band (L1 and L2) GNSS-Reflectometry and Microwave Radiometry [6], [7]. Notably, this mission was selected by the European Space Agency (ESA) for the second edition of its "Fly your Satellite!" program [8]. The Nadir Antenna is designed to radiate in axial mode and needs to be stowed in a small fraction of the 1U CubeSat. In addition, the antenna includes a tip mass (TM) at its far end to provide a gravity gradient effect that helps deliver nadir-pointing capability. Fig. 1 provides a rendering of the ^{3}Cat-4 orbiting the Earth in both its stowed and deployed configurations.

This work presents the design and optimization strategies of the ^{3}Cat-4 Nadir Antenna Deployment Subsystem (NADS). The Nadir Antenna forms a helix that is 68.1 mm in diameter and 506 mm in length, which greatly exceeds the 1U CubeSat's 100 mm x 100 mm x 100 mm dimensions. Furthermore, the stowed configuration of both the antenna and TM must be folded together inside the CubeSat frame, occupying just 26.8 mm in thickness. Therefore, the NADS's final design must provide an extreme packaging ratio —as small as 5%— as well as a stable, reliable, and highly scalable deployment mechanism for the antenna. This deployment system is considered by ESA as an enabling technology for future small satellite missions involving large helix antennas.

Several commercial helix antenna deployment systems for CubeSats currently exist. For example, in their GOMX-1 mission, GomSpace used a helix antenna in a 2U CubeSat to receive Automatic Dependent Surveillance-Broadcast (ADS-B) signals emitted by aircraft [9]. No details have been made available on this antenna deployment system design, but it is clearly less demanding than ours because the antenna is shorter, and must be stowed in a frame twice as big as ours.

Another example is a product from Helical Communication Technologies, who sell a Quadrifilar Helical Antenna that can operate from 400 MHz to 3000 MHz. The antenna

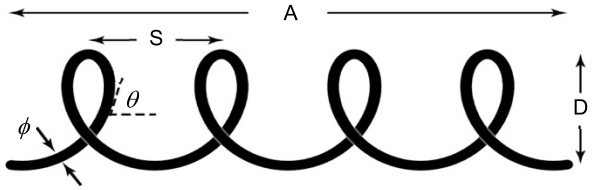

FIGURE 2. Helix geometry and main parameters.

is made from shape-memory alloy and, therefore, needs high levels of electric power. However, its dimensions are not compatible with our ^{3}Cat-4's requirements, since its compressed configuration occupies around 0.5U. Another important drawback to this antenna is its high price: around 12000 USD, as indicated on CubeSatShop website [10].

Some laboratory research work has also been done on helical antennas for CubeSats, such as the UHF quadrifilar helix antenna, UHF conical log spiral antenna, and Conical Log Spiral antenna that have been fabricated and tested by various laboratories [11], [12]. However, in terms of shape, size, and working frequency none of these options is compatible with a long helix in a 1U CubeSat. Nor can they accommodate a TM at the antenna's far end.

Consequently, it is clear that neither the commercial options nor those under research meet the NADS's demanding requirements. Our goal was to design a functional and highly stowable helix antenna with a low-shock and highly reliable deployment system. Additional requirements considered during the design phase were lightweight design, low power demand, affordability, and adaptability to different antenna configurations.

This paper is structured as follows. Section II of this paper presents the design of the Nadir Antenna and the results from our radiation model. Section III details the preliminary design of the main NADS mechanisms. Section IV presents our experimental methodology for obtaining two-dimensional accelerations of the antenna during deployment, and it further explains how this data was used to optimize the NADS's performance. In Section V, we present the results of the different tests conducted on the NADS's performance. Finally, our conclusions constitute the last section of this paper.

II. NADIR ANTENNA

The ^{3}Cat-4 Nadir Antenna is a tempered carbon steel helix designed to radiate at L-Band for GNSS-R and Radiometer experiments. This material was selected as a trade-off between RF characteristics and ease of manufacture. The helix turns fold counterclockwise, allowing for a highly directive antenna with left-hand circular polarization that, most importantly, can bestowed within a reduced space of 14 mm thickness. The antenna's radiofrequency characteristics are defined mainly by the helix parameters. Table 1 summarizes the nominal geometry of the helix, as defined in Fig. 2.

When operating, the Nadir Antenna must point toward the Earth (nadir direction). In order to help the magnetorquers

TABLE 1. Nominal geometry of the Nadir Antenna helix.

Symbol	Concept	Value
N	Number of turns [turns]	11
D	Diameter of the helix [mm]	68.1
ϕ	Section of the coil [mm]	1
S	Spacing between turns [mm]	46
θ	Pitch angle [º]	12.36
A	Total axial length (deployed) [mm]	506
a	Total axial length (stowed) [mm]	14

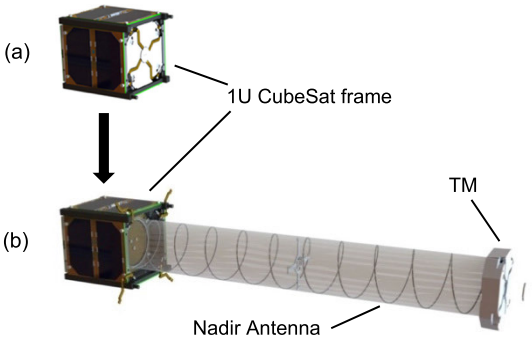

FIGURE 3. CAD model rendering of the Nadir Antenna and TM in stowed (a) and deployed (b) configurations.

that control attitude, a TM is attached to the external end of the antenna. This TM provides gravity-gradient stabilization with no energy needs (passive system) [13]. In the final design, the TM and the antenna weigh 100 gr and 28 gr, respectively. Fig. 3 shows a CAD model rendering of the antenna and TM in stowed and deployed configurations. The TM is designed to act as a retainer for the antenna in its stowed configuration, as the entire helix fits inside the hollow shape.

III. NADS PRELIMINARY DESIGN

A. DEPLOYMENT MECHANISM

The Nadir Antenna's helix behaves naturally like a spring. In its stowed configuration, it stores elastic potential energy that is transformed into kinetic energy once the helix is released. This means that the antenna deploys itself. We considered two main options for controlling this deployment: continuous release by a motor; or discontinuous release in several steps by melting dyneema strings.

The first option using a miniaturized motor provides fine control of the deployment velocity, but it requires considerably large space and high energy. It also increases the complexity of the mechanism without providing high levels of reliability, since the failure rate of miniaturized motors is non-negligible and redundancies are complex [14].

In the second option, the antenna is deployed by releasing the helix in several steps using dyneema strings. One end of each string is attached to the NADS structure, in contact with its corresponding melting and feedback circuitry on the NADS main board. The other end is attached to its corresponding step retainer, which is a solid piece placed at the section of the antenna that will be released in each step. In each step, the dyneema string is melted by the action of two redundant resistors, thus allowing for part of the helix to expand outward in its longitudinal direction. This system implies low power demand and operates by means of a simple mechanism. Moreover, the use of redundant melting circuit and a feedback system assures high reliability, which is crucial because the antenna constitutes a key instrument in achieving the mission objectives.

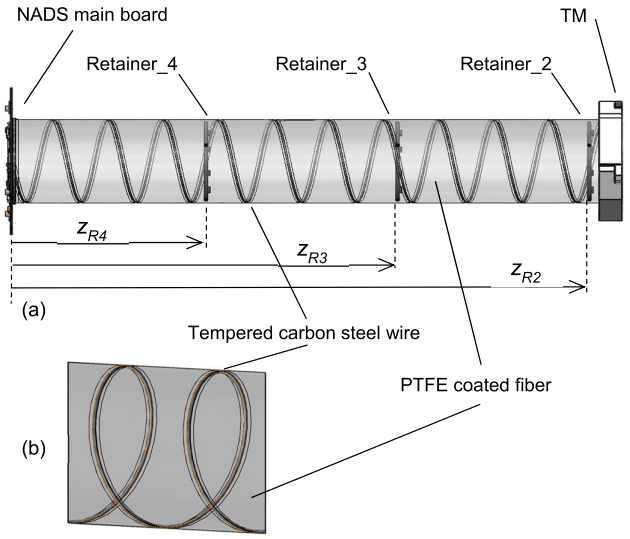

FIGURE 4. (a) CAD model of the NADS's main elements. Dyneema strings pull the retainers to the main board and release the corresponding step when they are melted. The longitudinal coordinates z_{Ri} are used in Section IV to optimize the length of each step. (b) Detail of the fiber coating sewn over the steel wire helix (gray strip), following the antenna's nominal geometry.

Therefore, after comparing the simplicity, cost, volume, and reliability of both systems, we chose the second option. Fig. 4 summarizes the NADS design, including the main board, the tempered carbon steel wire helix, the three retainers, the coated fabric, and the TM.

B. NOMINAL DIMENSIONS OF THE ANTENNA

Once the deployment system has been selected, it is necessary to find a way to ensure the nominal dimensions of the antenna in its deployed configuration. The diameter and distance between turns (pitch) of the helix must keep the exact values indicated in Table 1 in order to guarantee optimal antenna performance. However, the 1-mm tempered carbon steel wire is not rigid enough to maintain this desired helix shape by itself.

The first iteration of the design contemplated five parallel strips of fabric sewn over the antenna in the longitudinal direction while keeping the desired pitch between turns. The DLR used a similar concept for the AISat antenna design [15]. This solution was easy to implement but unpractical, since

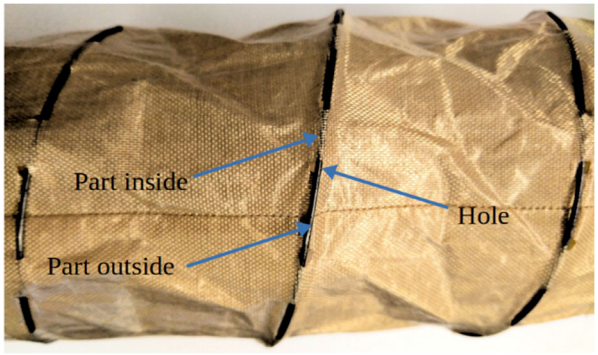

FIGURE 5. Picture of the attachment between the helical wire and the fabric. As it can be seen, the wire is introduced through holes following the helix geometry.

the sewn points between the fabric and the antenna tended to slip, thus altering the antenna's dimensions. To overcome this drawback, we ultimately selected a fabric that could be wrapped around the entire antenna, acting as a tensioned membrane structure. This design ensures the antenna's nominal diameter and pitch, since the tempered carbon steel wire is completely attached to the fabric and follows the desired path.

The fabric coating is attached to the helical wire as seen in Fig. 5. The wire is introduced through holes in the fabric, located all along the antenna path. Holes in the fabric following the desired helix path are made by laser cutting.

To maintain the tension of the coated fabric, the helix wire must be longer than the nominal length of the Nadir Antenna helix. In that way, the wire is slightly compressed inside the coated fabric and it therefore tightens the fabric by naturally pushing outward and against this resistance. On the other hand, the coating ensures that the antenna's nominal dimensions are maintained. The force, F, needed to extend or compress the helix wire by some distance, Δx, can be found by applying Hooke's law:

$$F = k\Delta x \tag{1}$$

where k is the stiffness of the spring, defined by its geometry and the wire's shear modulus of elasticity, G, which is given by the equation:

$$k = \frac{G\emptyset^4}{8ND^3} \tag{2}$$

The conducive wire material is tempered carbon steel ASTM A228, which has a $G = 210$ GPa. This results in a value of $k_S = 2.6$ N/m.

Taking into account that the real pitch of the wire in its relaxed state—when no force is applied—is constant, S_w, and that the fabric cover compresses it to the nominal pitch of the Nadir Antenna, $S_n = 46$ mm, each complete helix turn is compressed by a distance of ΔS, equal to the difference in pitch:

$$\Delta S = S_w - S_n = \Delta x/N \tag{3}$$

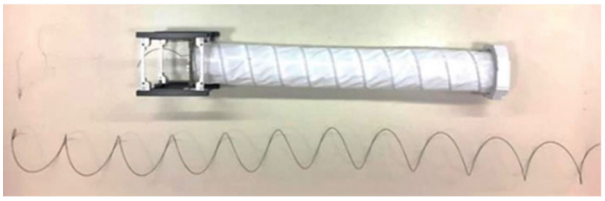

FIGURE 6. Picture of the Nadir Antenna compressed in the coated fabric (top) and relaxed (bottom).

Combining (1) and (3) and substituting $N = 11$ turns, the total force exerted by the spring when inside the coating can be found by:

$$F = k_H N \Delta S = 28.6\,(S_w - S_n) \tag{4}$$

The difference in pitch between the wire in its relaxed state and the compressed final configuration, $(S_w - S_n)$, must be large enough to ensure that the antenna tightens the fabric cover, but not so much as to compromise the structure.

Using (4), $S_w = 92$ mm has been selected. With this pitch, the total length of the helix wire is twice the nominal length of the Nadir Antenna (as can be seen in Fig. 6), and the force exerted by the spring when sewn to the coated fabric is $F = 1.316$ N.

The coated fabric must withstand the expected loads and deformations that the antenna will experience throughout the deployment phase and during its entire operational life. It also must be able to maintain its mechanical properties in the low Earth orbit environment, which is severely adverse due to ultraviolet radiation (UV), temperature effects, thermal cycling, and reactive atomic oxygen (atox) and O_2, in the atmosphere. From the Declared Material List (DML) approved by ESA [16], the most commonly used material for these kinds of applications is PTFE coated fiberglass [17]. PTFE coated fiberglass has a nominal thickness of 0.08 mm, a density of 155 gr/m2, an operational temperature range of between −73 °C and 288 °C, and a breaking strength in its fiber direction of 12259 N/m per width unit. This data clearly shows, the fabric cover is capable of withstanding a force of 2623 N, which is 9000 times greater than that exerted by the spring under static loading.

C. ANTENNA SECURITY LOCKING MECHANISM

The CubeSat's launching security protocols require that all stowed parts be held in place by a redundant system. That is why the whole system (Nadir Antenna + coated fabric + TM) is restrained in its stowed configuration by two redundantly secured dyneema strings that run from the NADS's aluminum case to the outer end of the TM.

When these two strings are melted by the action of two redundant resistors, the TM holder attached to the outer end of the TM is released, which then frees up four steel folder fingers that are locked into place until deployment is initiated. Upon release, these fingers rotate into their open position through the force of small axial springs attached to each

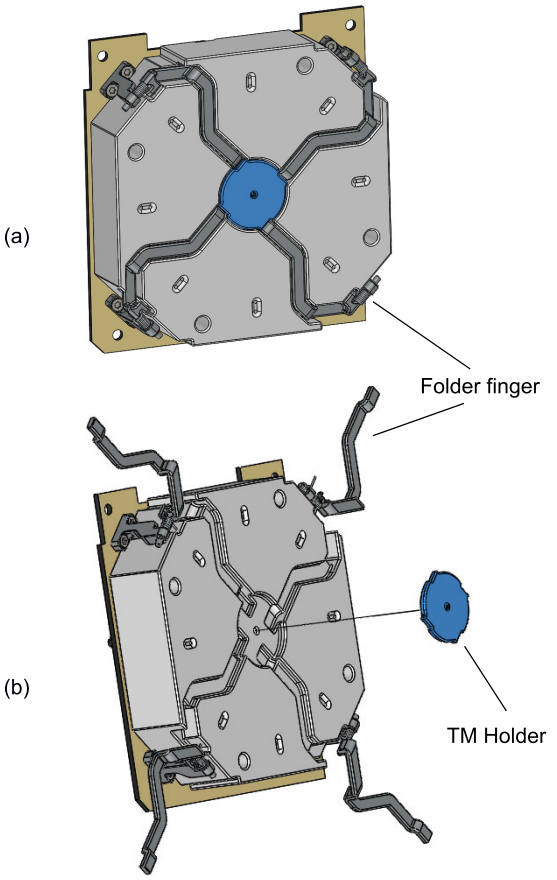

FIGURE 7. Picture of the Nadir Antenna compressed in the coated fabric (top) and relaxed (bottom).

finger's rotation axis, thus unlocking the TM. The fingers are designed in a curved shape so that they do not collide with the CubeSat structure when unfolded.

Fig. 7 depicts the main parts of the antenna's locking mechanism before and after melting the two secured dyneema strings.

Due to ESA's security protocols, the TM holder cannot be released into space. Therefore, a redundant nylon strings are needed for attaching the holder to the TM, with additional separation to ensure correct deployment (see Fig. 7 (b)).

IV. NADS OPTIMIZATION

A. EXPERIMENTAL MEASUREMENTS

The NADS is designed to deploy the antenna in several steps by successively melting dyneema strings. This chapter presents an exhaustive analysis of the effects that the number and length of these steps have on the deployment performance. Our study is relevant for two reasons: it helps determine the NADS's optimal configuration; and it also provides an experimental methodology for precisely measuring the kinematic characteristics of a deployment system. This second contribution is significant, since the applied methodology

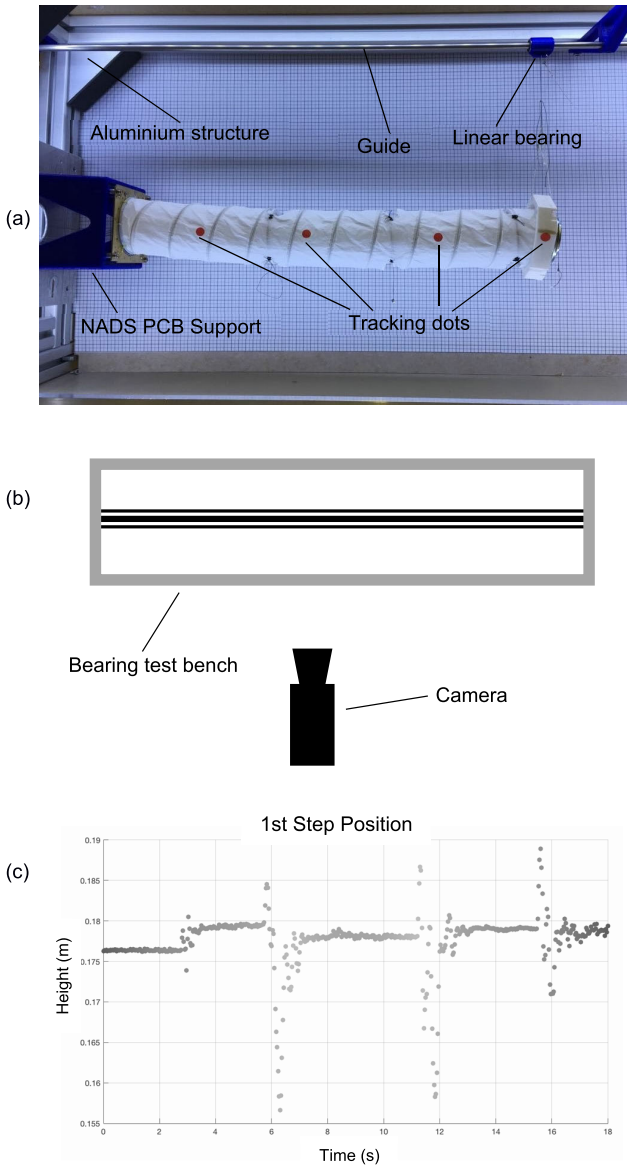

FIGURE 8. (a) Front picture of the bearing test bench used to test the NADS behavior. (b) Schematic front view of the bearing test bench and camera used to perform the measurements. (c) Tracking dot movement from one of the tests.

can be used in many different applications where the kinematic properties of a deployment system need to be found.

We performed the experimental measurements using the bearing test bench shown in Fig. 8 (a). It is composed of an aluminum structure, a support for the NADS printed circuit board (PCB) and a guide for moving the bearing line attached to the TM. A pulley with a small weight helps overcome the bearing line's static frictional force during deployment. The antenna deployment direction is horizontal, while the disturbances we aim to measure are its small vertical displacements (bending).

The data acquisition system is illustrated in Fig. 8 (b) and consists of a slow-motion camera placed on a tripod in front

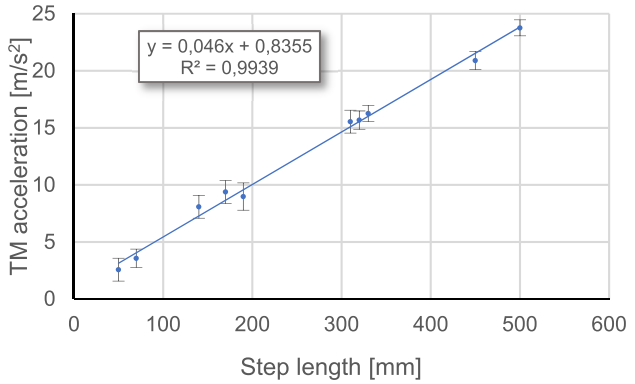

FIGURE 9. Acceleration of the TM for different single step lengths.

of the test bench. Tracking dots are painted in red at the analysis points along the antenna and the side of the TM (see Fig. 8 (a)). During deployment, the camera recorded the movement of the tracking dots. Image recognition software was able to track the vertical position of these dots at any time, as shown in Fig. 8 (c). The two-dimensional velocity and acceleration of the different antenna sections were calculated from the change in position of the red points between successive frames, Δd, and the camera frame rate.

B. NUMBER OF STEPS

The two study variables are: the TM's acceleration in the axial direction, a; and the bending of the antenna, this being the antenna's off-axis displacement during deployment, due to asymmetries in mass, geometry, and forces.

As the number of steps increases, the acceleration and of the antenna decreases during each step of the deployment, resulting in smoother movement. However, not more than three retainers can be used, because their thickness would make it impossible to compress the whole antenna and TM within the desired space. Therefore, this optimization incorporates a maximum of four steps: one step for each of the three retainers; and a fourth one for the TM (see Fig. 4).

Fig. 9 shows the accelerations obtained on the bearing test bench for single step lengths of 50, 70, 140, 170, 190, 310, 320, 330, 450 and 500 mm. The experimental results show that the TM acceleration increases linearly with step length, with the ratio between them being equal to 46.0 $1/s^2$. This is consistent with Hooke's law, which predicts, first, that the TM's acceleration is lowest for the shortest deployment length and, second, that the added total accelerations in all steps remain constant. From these results, it is clear that equispaced steps assure minimum acceleration in each single step. Therefore, if contemplating only TM acceleration, the optimal NADS configuration would comprise four steps measuring 126.6 mm each. In this design, Retainer_4 would be placed at $z_{R4} = 126.6$ mm, Retainer_3 at $z_{R3} = 253.2$ mm, and Retainer_2 at $z_{R2} = 379.8$ mm.

However, antenna bending must also be taken into account. Indeed, non-axial deformations during deployment can affect the dynamics of the entire satellite and, even more importantly, lead to catastrophic impact of the TM against the solar panels located on the CubeSat's sides.

TABLE 2. Maximum bending averaged from five tests in eight different NADS configurations—from four to a single step. This data provides a total bending average for each number of steps.

Steps	Configuration	Max. Bending average [mm]
Four Steps	TMS-2S-3S-4S	63
Three Steps	TMS-2S-3S	91
	TMS-2S-4S	65
	TMS-3S-4S	57
Two Steps	TMS-2S	133
	TMS-3S	63
	TMS-4S	35
One Step	TMS	124

C. STEP SIZE

To understand the effect of step size on the bending of the antenna, we performed tests for deployments of four, three, two and one single steps. For each of these configurations, different step lengths were compared. In space, bending can appear during deployment in any off-axis direction (3D movement), and it can be caused either by mass/geometry asymmetries in the compressed positioning of the antenna or by rotational velocity during deployment. In order to experimentally simulate these disturbances in the laboratory (2D movement), the effect of Earth's gravity on the deployment dynamics can be used to force bending to occur in the vertical direction (downward). In that way, maximum bending, y_B, is measured as the maximum vertical deviation of the antenna as seen from the slow-motion camera.

Table 2 summarizes the different combinations tested on the bearing test bench, as well as the maximum bending measured for every possible configuration. The table refers to the tip mass, second, third and fourth steps as, respectively: TMS, 2S, 3S and 4S. Each value in the table is the obtained average of five different tests. As expected, the bending average is reduced when the number of steps increases to four. The worst-case scenario is the single step deployment, where a maximum bending of 124 mm was measured. In contrast, the four-step configuration leads to a maximum bending of 63 mm. Looking at the three- and two-step configurations, it is clear that bending values grow smaller as the retainers are located closer to the CubeSat frame.

Based on these general results, the optimal length of the four steps can be calculated by finding the overall configuration that minimizes acceleration and bending during the entire deployment maneuver. To that end, we have conducted tests with different retainer positions.

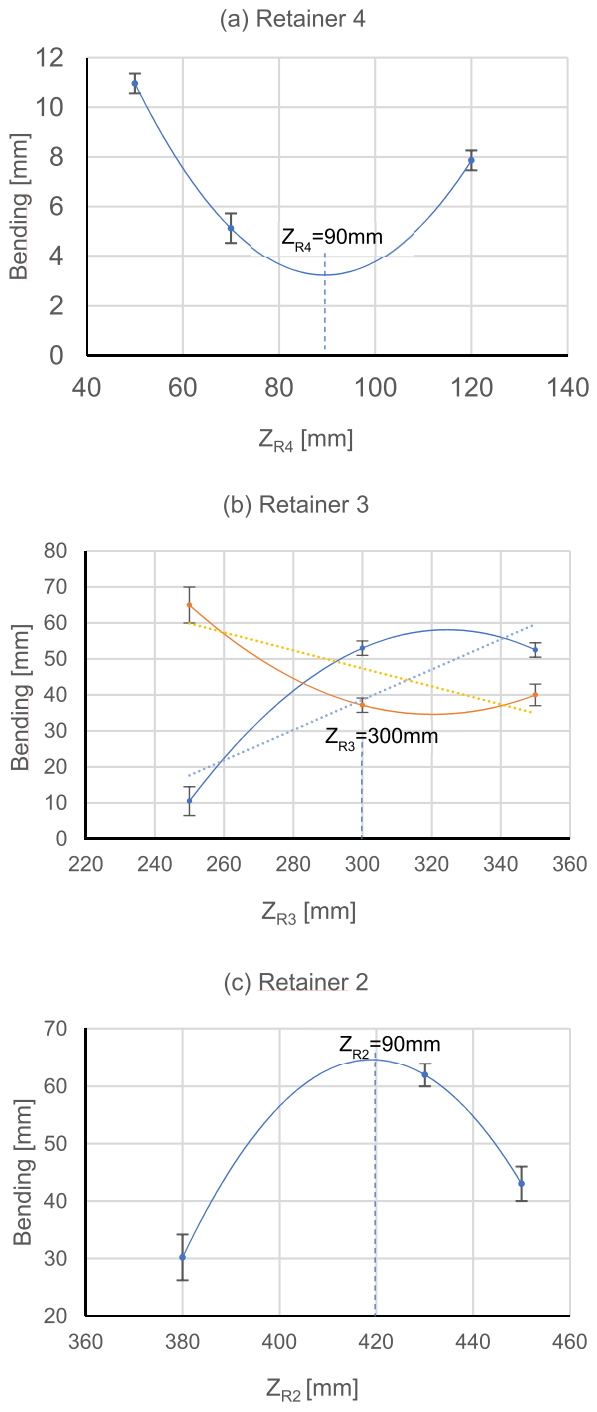

FIGURE 10. Maximum bending distances as a function of the positions of Retainer_3 (a), Retainer_2 (b) and Retainer_1 (c). Each point in the graphs is an average of five measurements.

Fig. 10 (a) shows the maximum bending distance as a function of Retainer_4 distance to the NADS main board, z_{R4}. Retainer_4 is the attachment point of the last melted string, which means that these tests were performed with the rest of the antenna already deployed. That is the reason why the maximum bending distance increases from 5.1 mm to 10.9 mm when the retainer is moved from 70 mm to 50 mm. Using a quadratic interpolation, a minimum bending of 3.2 mm is obtained when Retainer_4 is located at $z_{R4} = 90$ mm.

To find the optimal position of Retainer_3, additional deployments are analyzed for z_{R3} equal to 250, 300 and 350 mm. In this case, we measure the bending distances of the second and third steps because Retainer_3 affects both. Fig. 10 (b) shows the maximum bending distance of the second and third steps (blue and orange lines, respectively) as a function of the Retainer_3 position. Linear and quadratic interpolations are used in both stages, and the optimum position of the retainer is determined by the intersection of both interpolations. Logically, as the retainer moves away from the CubeSat frame, third-stage bending increases and second-stage bending is reduced. The two interpolations give us an optimum interval for z_{R4} that is located between 290 mm and 310 mm. Therefore, Retainer_3 is ultimately placed at 300 mm.

Finally, the optimal position of Retainer_2 is calculated using the data obtained from a new set of tests. As shown in Table 2, bending is reduced by moving the retainers closer to the CubeSat frame. However, in this case it is desirable to ensure a short TM step in order to prevent the TM from causing any damage to the CubeSat frame during deployment. Thus, the tested z_{R2} values are 380, 430, and 450 mm. Fig. 10 (c) shows that the maximum bending is obtained when z_{R2} is 420 mm. In this case the minimum values occur at both ends of the selected range. Keeping in mind that a short TM step is mandatory, Retainer_2 is placed at 420 mm.

In summary, the deployment of the antenna is composed of four steps, divided by three retainers. Our experimental methodology has allowed us to find the optimal position of these retainers: $z_{R4} = 90$ mm, $z_{R3} = 300$ mm and $z_{R2} = 420$ mm.

V. NADS VERIFICATION AND VALIDATION

A. VALIDATION

To validate the mechanical behavior of the Nadir Antenna and NADS performance, a series of tests must be performed. First, antenna rigidity must be characterized. Then, a long-term test is needed to guarantee that the helix shape is not altered after several months in its stowed configuration. Finally, thermal vacuum tests will prove proper performance of the NADS mechanism.

B. RIGIDITY CHARACTERIZATION

The ^{3}Cat-4 attitude control subsystem uses 3 axis magnetorquers to generate torques and orient the satellite so that the antenna is nadir-pointing. These torques are produced near the structure's geometric center, and they could impose non-desirable accelerations while causing deformations at the antenna's far end as well as to the TM. Using the bearing test bench, a small force can be applied perpendicularly to the antenna while increasing this force in increments of 0.002 N, thus allowing us to measure the TM's linear and angular

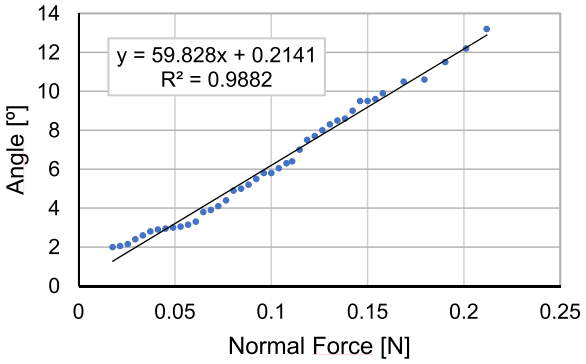

FIGURE 11. Nadir Antenna's angular deformation caused by the action of a normal force.

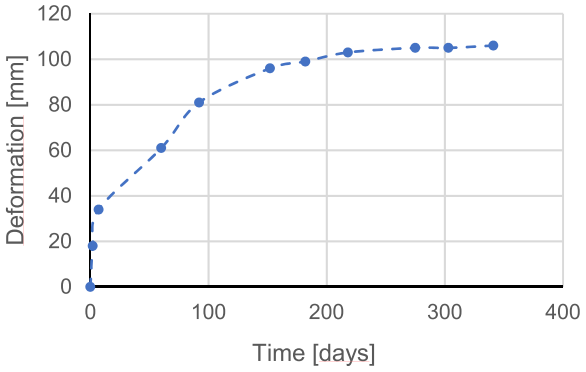

FIGURE 12. Permanent deformation of the helix steel wire as a function of the full compression time.

deformations. Fig. 11 presents the linear relationship between the antenna's angular deformation and the perpendicular force applied to the TM.

The CubeSat's expected maximum angular acceleration once in orbit is set to $\alpha = 3.84{\cdot}10^{-3}$ rad/s. The force exerted on the TM by this angular acceleration can be calculated using:

$$F = Md\alpha \tag{5}$$

where $M = 0.120$ kg is the TM mass (masses of the antenna and coated fabric assumed to be negligible) and $d = 0.53$ m is the distance between the CubeSat's geometric center and the TM. Using these values, a maximum force of $2.44{\cdot}10^{-4}$ N is obtained. By substituting this with the experimental result in Fig. 11, the maximum expected angular deformation of the TM is smaller than 1° and, therefore, negligible for the mission goals.

To analyse the dynamic response of the antenna due to the excitations applied by the magnetorquer, we experimentally measured the spring constant for lateral vibrations. From this, the natural frequencies of the lateral oscillations are calculated, with the highest one being equal to 0.55 Hz. This value is almost four times smaller than the attitude actuators' minimum refresh rate of 2 Hz, meaning that there will be no coupling between the actuators and the antenna.

C. LONG-TERM TEST

This test is crucial for verifying that the helix antenna does not lose its elastic properties, even after having been fully compressed in its stowed configuration for the maximum design time of 12 months (test campaign + waiting period before launch + security margin). To verify the elastic properties, the length, L, and the stiffness, k, of the helix are measured before and after the stowed period.

The test was performed by keeping the tempered carbon steel wire —without the coated fabric and TM— fully compressed for one day, one week, one month, and every month consecutively up to a whole year. We then analyzed the differences between the initial helix length and that which was measured after compression. Fig. 12 presents the permanent deviation measured during the long-term test, as a function of the time during which the helix wire was fully compressed. Deformations were notable during the first few days. After one week of compression, the helix length was reduced by 39 mm, 3.8% of the initial value. However, this trend changed as compression time increased, leading to permanent deformations of 86.1 mm and 106 mm after 92 days and 341 days, respectively. This last value means that, after almost a year of full compression, the helix size was reduced only 10%.

The evolution of the helix stiffness can be calculated using experimental data measured by a dynamometer. During the deformation tests explained directly above, we measured the helix elongations when different forces were applied. The stiffness is the ratio between the applied force and the elongation, and a constant value of $k = 0.3$ N/m is obtained

Considering the 10% permanent plastic deformation of the spring length, we can redo the calculations carried out in section II.B. Using Equation 4, the new force exerted by the spring when sewn to the coated fabric is 1.052 N. From this result, it is clear that, even after a long period of full compression, the helix wire maintains its elastic properties and can be deployed normally.

D. THERMAL VACUUM TESTS

The NADS was tested in a thermal vacuum chamber (TVAC) at ESEC Galaxia Cleanroom (ESA facilities) [18]. The test was performed in cold conditions, since these represent the most critical scenario in terms of temperature stress. The deployment occurs when the burning resistor burns the dyneema melting string, thus releasing part of the antenna. Having the resistor and the melting string in extreme cold conditions can be critical, since the resistor must be able to provide a high enough temperature to melt the string. Moreover, there exists the possibility that the antenna sheath could be stiff at cold temperatures, preventing it from a successful deployment.

The test was performed at qualification level, meaning that only 5 °C of margin was taken from the operational temperature of the subsystem. Thus, we tested the subsystem

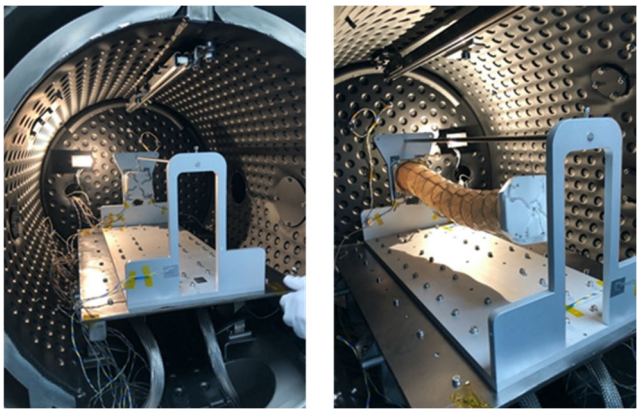

FIGURE 13. Pictures of the NADS TVAC test set-up. (a) Before the test and (b) after the antenna deployment. Test conditions are −35 °C and $0.2 \bullet 10^{-5}$ Pa.

at −35 °C with a dwell time of 1 hour to stabilize the temperature. Chamber pressure was lowered to $0.2 \cdot 10^{-5}$ Pa.

After an additional 15 minutes (plateau phase), the Nadir Antenna deployed successfully, which we determined by performing a visual inspection while the antenna was inside the TVAC and by measuring the length of the antenna once the TVAC was pressurized and opened. Figure 13 shows the interior of the TVAC at the ESEC Galaxia Cleanroom, where we can see the NADS in both its stowed and deployed configurations after the successful deployment.

A thermal analysis was performed to study the hot case, where dyneema strings may melt due to extreme heat. A maximum temperature of +45 °C was determined, thus validating the thermal behavior of the subsystem.

E. FABRIC TEMPERATURE TEST

ESA Academy supervisors expressed some concern about the coated fabric's mechanical behavior under the mission's extreme temperatures. Thus, we carried out a test to verify the resistance of the NADS coated fabric. A force of 3 N (four times the maximum expected force) was applied to the piece of fabric under a pressure of 10^{-4} Pa and temperatures of −73 °C and −100 °C. The objective was to reach the lowest possible temperature using the TVAC in order to reach the limits indicated on the fabric datasheet and check its mechanical behaviour. The fabric withstood the applied force during the test and was able to successfully pass a traction test once extracted from the TVAC. These results were considered satisfactory by ESA Academy supervisors. Fig 14 shows the fabric temperature test set-up.

VI. RADIATION PERFORMANCE

We measured a prototype of the Nadir Antenna in an anechoic chamber and obtained metrics for directivity and the front-to-back lobe ratio (FBR). Figure 15 shows the radiation patterns obtained in the anechoic chamber. The diagrams are normalized and linear, not in dBs.

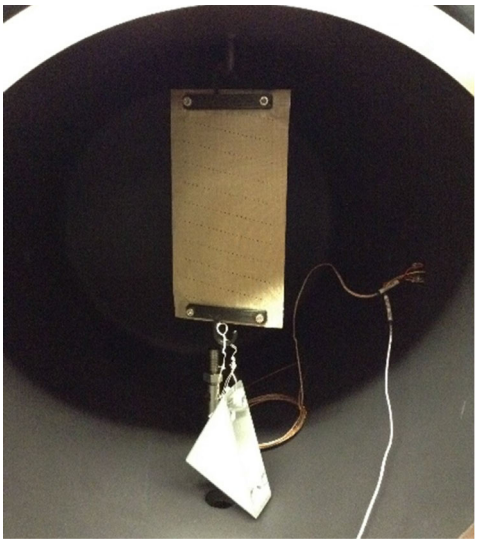

FIGURE 14. Fabric temperature test set-up. Test conditions are 10^{-4} Pa and temperatures of −73 °C and −100 °C.

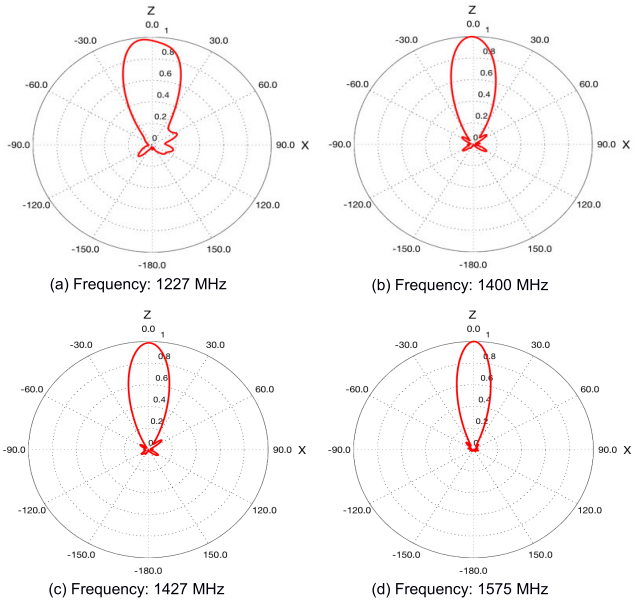

FIGURE 15. Nadir Antenna's radiation patterns for (a) 1227 MHz, (b) 1400 MHz, (c) 1427 MHz, (d) 1575 MHz. Diagrams are normalized and linear, not in dBs.

Table 3 includes the resultant directivity, FBR, and return loss (S11) as a function of frequency.

The matching for the NADS antenna is complex, since it covers a wide range of frequencies, from 1227 MHz up to 1575 MHz. According to the mission requirements, the return loss should be less than -15 dB at 1400 up to 1427 MHz and less than -10 dB at 1227 MHz and 1575 MHz. However, in the qualification model the results obtained were higher in some bands, as seen in Table 3 and Fig 16. The flight model (FM) will address this discrepancy by means of a manual matching

TABLE 3. Nadir Antenna's directivity, FBR, and return loss (S11) as a function of frequency.

Frequency (MHz)	Directivity (dB)	FBR (dB)	S11 (dB)
1227	7.49	5.70	-22.59
1400	9.43	15.46	-12.13
1427	10.52	17.39	-11.97
1575.42	11.44	16.8	-8.84

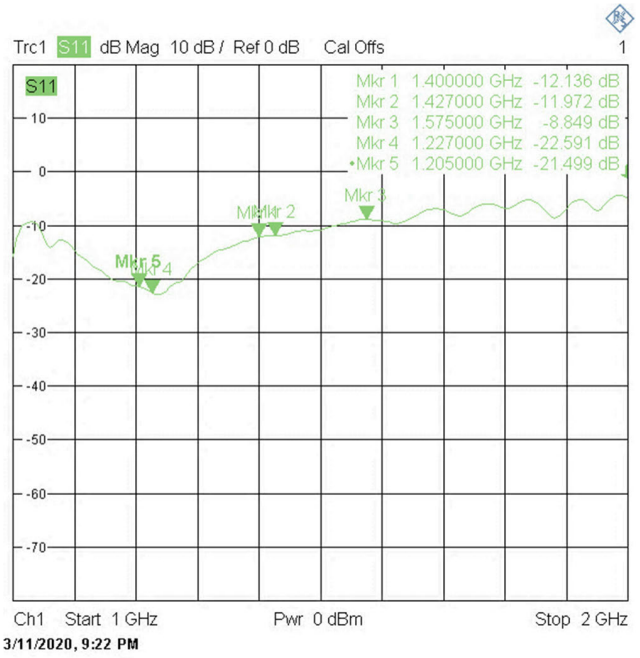

FIGURE 16. Nadir antenna matching (S11).

technique to move the peak currently located at 1227 MHz to the 1400 MHz to 1427 MHz band.

No simulations were conducted to characterize the antenna performance of this engineering model (EM) because some elements are difficult to characterize, such as the antenna fabric and other mechanical elements. Nevertheless, the team is currently working on implementing the flight model (FM) and, once it is done, the antenna performance and its effect on the satellite will be fully characterized. All this future work will be included in an article about the antenna performance, including on-ground measurements, simulations, and In-Orbit Validation data.

VII. CONCLUSION

This article describes the design of a deployment system for a 506-mm-long helix antenna attached to a single 1U CubeSat. The proposed deployment system is divided into four steps, each triggered by melting a dyneema string. It also contains an antenna security locking mechanism to ensure it is held in place by a redundant system before deployment. The results from a set of tests demonstrate that the deployment system has excellent performance, both mechanically and from the electromagnetic points of view. Therefore, the deployment system has proved to be completely functional while also being an affordable and reliable design that can be used in many different mechanisms. This article also contributes a methodology for optimizing the different step lengths by measuring the kinematic characteristics of each deployment step.

REFERENCES

[1] S. Rodriguez-Donaire, M. Sureda, D. Garcia-Alminana, E. Sierra, J. S. Perez, P. C. Roberts, J. Becedas, G. H. Herdrich, D. Kataria, R. Outlaw, and L. Ghizoni, "Earth observation technologies: Low-end-market disruptive innovation," in *Satellites and Innovative Technology*. London, U.K.: InTech, 2020.

[2] J. Nieto *et al.*, "Large deployable offset fed antennas for CubeSats," in *Proc. 40th ESA Antenna Workshop*, 2019.

[3] Y. Rahmat-Samii, V. Manohar, and J. M. Kovitz, "For satellites, think small, dream big: A review of recent antenna developments for CubeSats," *IEEE Antennas Propag. Mag.*, vol. 59, no. 2, pp. 22–30, Apr. 2017.

[4] H. King and J. Wong, "Characteristics of 1 to 8 wavelength uniform helical antennas," *IEEE Trans. Antennas Propag.*, vol. AP-28, no. 2, pp. 291–296, Mar. 1980.

[5] *The CubeSat Program, Cal Poly SLO. CubeSat Design Specification*, California Polytech. State Univ., San Luis Obispo, CA, USA, 2009.

[6] J. F. Munoz-Martin, N. Miguelez, R. Castella, L. Fernandez, A. Solanellas, P. Via, and A. Camps, "3Cat-4: Combined GNSS-R, L-Band radiometer with RFI mitigation, and AIS receiver for a I-unit CubeSat based on software defined radio," in *Proc. IGARSS-IEEE Int. Geosci. Remote Sens. Symp.*, Valencia, Spain, Jul. 2018, pp. 22–27.

[7] J. A. Ruiz-de-Azua, M. Sobrino, A. Navarro, H. Lleo, M. Sureda, M. Soria, A. Calveras, A. Camps, J. F. Munoz, L. Fernandez, M. Badia, D. Llaveria, C. Diez, A. Aguilella, A. Perez, and O. Milian, "3Cat-4 mission: A 1-unit CubeSat for Earth observation with a L-band radiometer and a GNSS-reflectometer using software defined radio," in *Proc. IGARSS-IEEE Int. Geosci. Remote Sens. Symp.*, Jul. 2019, pp. 8867–8870.

[8] *ESA Academy—Fly Your Satellite! Programme*. Accessed: Jan. 27, 2020. [Online]. Available: https://www.esa.int/Education/CubeSats_-_Fly_Your_Satellite/Fly_Your_Satellite!_programme

[9] L. K. Alminde, J. Christiansen, K. K. Laursen, A. Midtgaard, M. Bisgaard, M. Jensen, B. Gosvig, A. A. Birklykke, P. Koch, and Y. L. Moullec, "GomX-1: A nanosatellite mission to demonstrate improved situational awareness for air traffic control," in *Proc. 26th Annu. AIAA/USU Conf. Small Satellites*, 2012, pp. 1–17.

[10] *CubeSat Shop—Helios Deployable Antenna*. Accessed: Feb. 11, 2020. [Online]. Available: https://www.cubesatshop.com/product/helios-deployable-antenna/

[11] J. Costantine, Y. Tawk, I. Maqueda, M. Sakovsky, G. Olson, S. Pellegrino, and C. G. Christodoulou, "UHF deployable helical antennas for CubeSats," *IEEE Trans. Antennas Propag.*, vol. 64, no. 9, pp. 3752–3759, Sep. 2016.

[12] A. J. Ernest, Y. Tawk, J. Costantine, and C. G. Christodoulou, "A bottom fed deployable conical log spiral antenna design for CubeSat," *IEEE Trans. Antennas Propag.*, vol. 63, no. 1, pp. 41–47, Jan. 2015.

[13] P. Dow, F. Scammell, F. Murray, N. Carlson, and I. Buck, "Dynamlc stability of a gravity gradient stabilized satellite having long flexible antennas," in *Proc. Guid. Control Conf.*, Seattle, WA, USA, Aug. 1966, pp. 285–303.

[14] P. Hoehn, "Design, construction and validation of an articulated solar panel for CubeSats," in *Proc. 29th Annu. AIAA/USU Conf. Small Satell.* Logan, UT, USA: Utah State Univ., 2015, pp. 69–78.

[15] T. Sproewitz, J. Block, A. Bager, L. Hauer, and M. Schuetze, "Deployment verification of large CFRP helical high-gain antenna for AIS signals," in *Proc. Aerosp. Conf.*, Big Sky, MT, USA, Mar. 2011, pp. 5–12.

[16] *Space Product Assurance—Data for Selection of Space Materials and Processes*, Standard ECSS Q70-71A, 2004.

[17] NASA. *Tensile Fabrics Enhance Architecture Around the World*. Accessed: May 31, 2019. [Online]. Available: https://spinoff.nasa.gov/Spinoff2009/ip_2.html

[18] *ESA Galaxia*. Accessed: Apr. 12, 2020. [Online]. Available: https://www.esa.int/Education/Galaxia_a_new_boost_for_ESA_Education

MIQUEL SUREDA was born in Barcelona, Spain, in 1978. He received the bachelor's degree in physics from the University of Barcelona, Barcelona, in 2001, and the bachelor's and master's degrees in aerospace engineering from the Polytechnic University of Madrid, Madrid, Spain, in 2007, and the Ph.D. degree from the Technical University of Catalonia–BarcelonaTech (UPC), Barcelona, in 2012.

Since 2007, he has been a full-time Lecturer with the Technical University of Catalonia–BarcelonaTech (UPC). Since 2017, he has also been collaborated with the Nanosat Lab (UPC), mainly involved in the 3Cat-4 Project, within ESA's ''Fly Your Satellite!'' Program. He is also the part of the H2020 Project DISCOVERER, devoted to develop new technologies to revolutionize earth observation by operating satellites at very low earth orbits. His research interests include electric space propulsion systems and spacecraft design. His current research interests include the design and optimization of interplanetary missions and sustainable offworld settlements.

Dr. Sureda is a member of the Board of the Sustainable Offworld Network (SONet), a community of professionals in the academic and private sectors dedicated to the development of sustainable human settlements on other worlds, especially on the Moon and the Mars.

MARCO SOBRINO was born in Barcelona, Spain. He received the Engineering degree in industrial technologies from the Technical University of Catalonia–BarcelonaTech (UPC), Barcelona, Spain, in 2018, where he is currently pursuing the master's degree in industrial engineering.

He has participated in several student projects related to stratospheric balloons and life support systems. He is also participating in the development of the CubeSat 3CAT-4 within ESA's ''Fly Your Satellite!'' Program and the RITA payload in the UAE GRSS, as a Mechanical Engineer. His research interests include the design, manufacturing, and analysis of satellite structures and mechanisms, additive manufacturing, and generative design.

ORIOL MILLAN was born in Barcelona, Spain. He is currently pursuing the Engineering degree in industrial technologies engineering with the Technical University of Catalonia–BarcelonaTech (UPC), Barcelona, Spain.

Since 2018, he has been a member of the NanoSat Lab, mainly working in the development of the NADS subsystem for the mission 3Cat4 part of the ESA's ''FlyYourSatellite!'' Program.

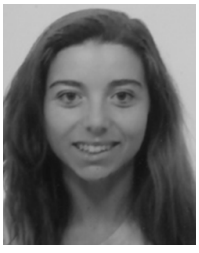

ANDREA AGUILELLA was born in A Coruña, Spain. She received the degree in industrial technologies engineering from the Universidade de Vigo, Galicia, Spain, in 2016, and the M.S. degree in industrial engineering, specialized in mechanics from the Technical University of Catalonia–BarcelonaTech (UPC), Barcelona, Spain, in 2020.

She is working in the management of R&D projects at FI Group Company. She has participated in the ''Fly Your Satellite!'' Program from the ESA, and the FSSCat Project, which is the Winner of the ESA Sentinel Small Sat^3 Challenge of the Copernicus Masters Competition. Her research interests include the satellite structures and mechanisms, specially the satellite deployment systems, and the simulation tools oriented to design.

ARNAU SOLANELLAS was born in Tarragona, Spain. He received the bachelor's and M.Sc. degrees in electronic engineering from the Technical University of Catalonia–BarcelonaTech (UPC), Barcelona, Spain, in 2016 and 2020, respectively.

He was involved at the NanoSat Lab (UPC), within ESA's ''Fly Your Satellite!'' Program. He is currently working at Ingenia Motion Control, Barcelona, Spain, as a Power Electronics Engineer. His research interests include power efficiency, power electronics miniaturization, electromagnetic compatibility, and thermal design applied to electronics.

MARC BADIA was born in Berga, Spain. He received the degree in electronics systems of telecommunications engineering from the Technical University of Catalonia–BarcelonaTech (UPC), Barcelona, Spain, in 2018, where he is currently pursuing the M.Sc. degree in electronics engineering.

He has participated in the FSSCat Project, which is the Winner of the ESA Sentinel Small Sat S^3 Challenge of the Copernicus Masters Competition. He is currently participating in the ''Fly your Satellite!'' Program from the ESA. He is a member of the RITA Payload Team in the Second GRSS Student Grand Challenge.

JOAN FRANCESC MUNOZ-MARTIN was born in Mallorca, Spain, in 1992. He received the M.Sc. degree in telecommunications engineering from the Technical University of Catalonia–BarcelonaTech (UPC), Barcelona, Spain, where he is currently pursuing the Ph.D. degree.

In 2013, he joined the NanoSat Lab, as a Communications System Engineer, for the 3Cat-1 mission and has been involved in all its missions ever since. He participated in ESA's BEXUS 19 Campaign, with a proof of concept of the GNSS-R spaceborne technology integrated in 3Cat-2. He also led the OBDH, TT&C, and ground operations for 3Cat-2 mission. He is the Lead Software and Payload Engineer with 3Cat–4 mission, part of ''Fly Your Satellite!'' Program from the ESA. Moreover, he is the Payload Manager of the GNSS-R and L-band radiometer microwave passive payload of the ESA S3 FSSCat mission. In addition, he is responsible for the circular polarization GNSS-R experiment of the MOSAiC campaign in the arctic sea.

LARA FERNANDEZ (Student Member, IEEE) was born in Barcelona, Spain. She received the bachelor's and M.Sc. degrees in telecommunications engineering from the Technical University of Catalonia–BarcelonaTech (UPC), Barcelona, Spain, in 2017 and 2019, respectively, where she is currently pursuing the Ph.D. degree.

She is also participating in the ''Fly Your Satellite!'' Program from ESA, and a member of the FSSCat Project, which is the Winner of the ESA Sentinel Small Sat S^3 Challenge of the Copernicus Masters Competition. Her research interests include the Internet of Things, 5G networks, satellite networks, communication systems, and antenna design.

JOAN A. RUIZ-DE-AZUA (Member, IEEE) was born in Barcelona, Spain. He received the degree in aerospace engineering from Supaero, Toulouse, France, and in telecommunications engineering from the Unversitat Politècnica de Catalunya, Barcelona, Spain, in 2015, and the M.S. degree in network protocols from Supaero, in 2015. He is currently pursuing the Ph.D. degree with the Universitat Politècnica de Catalunya.

He has participated in different projects of ground segment for Ariane 5 and Ariane 6 programs at GTD Company, in collaboration with CNES and ESA. He is currently participating in the "Fly Your Satellite!" Program from ESA, and a member of the FSSCat Project, which is the Winner of the ESA Sentinel Small Sat S^3 Challenge of the Copernicus Masters Competition. His research interests include satellite architectures, satellite networks, cognitive networks, the Internet of Things, 5G networks, deep learning, and embedded software. He was awarded with the best M.S. thesis on critical communications from the Official Spanish Telecommunications Chartered Institute, in 2016.

ADRIANO CAMPS was born in Barcelona, Spain, in 1969. He received the degree in telecommunications engineering and the Ph.D. degree in telecommunications engineering from the Technical University of Catalonia–BarcelonaTech (UPC), Barcelona, Spain, in 1992 and 1996, respectively.

In 1991 to 1992, he was at the ENS des Télécommunications de Bretagne, France, with an Erasmus Fellowship. Since 1993, he has been with the Electromagnetics and Photonics Engineering Group, Department of Signal Theory and Communications, UPC, where he was first an Assistant Professor and an Associate Professor, in 1997, and has also been a Full Professor, since 2007. In 1999, he was on sabbatical leave at the Microwave Remote Sensing Laboratory, University of Massachusetts at Amherst, Amherst. Since 1993, he has been deeply involved in the European Space Agency SMOS Earth Explorer Mission from the instrument and algorithmic points of view, performing field experiments, and studying the use of GNSS-R techniques to perform the sea state correction needed to retrieve salinity from L-band radiometric observations, since 2001. He has advised 23 Ph.D. thesis students (+8 on-going) and more than 120 final projects and M.Eng. theses. He has published over 203 articles in peer-reviewed journals, six book chapters, one book, and more than 425 international conference presentations, and holds 12 patents. His research interest includes microwave remote sensing, with special emphasis in microwave radiometry by aperture synthesis techniques and remote sensing using signals of opportunity (GNSS-R).

Dr. Camps's publications have received more than 6347/9547 citations, and his H-index is 38/47 according to Scopus/Google Scholar, according to Publish or Perish (Google Scholar).